AGU PUBLICATIONS

JGR

Journal of Geophysical Research: Oceans

RESEARCH ARTICLE

10.1002/2016JC012664

Special Section:
Dense water formations in the North Western Mediterranean: From the Physical Forcings to the Biogeochemical Consequences

Key Points:
- NW Mediterranean zonation based on nutrients during convection event, and based on fluorescence profiles during bloom
- Convection spatial scale drives the nutrients distribution and mixing depth drives the nutrient stoichiometry
- Winter nutrient supply drives spring phytoplankton distribution while stoichiometry drives community structure

Supporting Information:
- Supporting Information S1

Correspondence to:
T. Severin,
tatiana.severin@austin.utexas.edu;
F. Kessouri,
kesf@ucla.edu

Citation:
Severin, T., et al. (2017), Open-ocean convection process: A driver of the winter nutrient supply and the spring phytoplankton distribution in the Northwestern Mediterranean Sea, *J. Geophys. Res. Oceans*, *122*, 4587–4601, doi:10.1002/2016JC012664.

Received 27 DEC 2016
Accepted 4 MAY 2017
Accepted article online 12 MAY 2017
Published online 3 JUN 2017

Open-ocean convection process: A driver of the winter nutrient supply and the spring phytoplankton distribution in the Northwestern Mediterranean Sea

Tatiana Severin[1,2], Faycal Kessouri[3,4], Mathieu Rembauville[1], Elvia Denisse Sánchez-Pérez[1], Louise Oriol[1], Jocelyne Caparros[1], Mireille Pujo-Pay[1], Jean-François Ghiglione[1], Fabrizio D'Ortenzio[5], Vincent Taillandier[5], Nicolas Mayot[5], Xavier Durrieu De Madron[6], Caroline Ulses[3], Claude Estournel[3], and Pascal Conan[1]

[1]Laboratoire d'Océanographie Microbienne (LOMIC), Observatoire Océanologique, Sorbonne Universités, CNRS, UPMC Univ Paris 06, CNRS, Banyuls/Mer, France, [2]Now at Marine Science Institute, The University of Texas at Austin, Port Aransas, Texas, United States, [3]Laboratoire d'Aérologie, CNRS, Université de Toulouse, Toulouse, France, [4]Now at Department of Atmospheric and Oceanic Sciences, University of California Los Angeles, Math Sciences, Los Angeles, California, United States, [5]Sorbonne Universités, UPMC Univ Paris 06, INSU-CNRS, Laboratoire d'Océanographie de Villefranche (LOV), Villefranche-sur-mer, France, [6]CEFREM, CNRS-Université de Perpignan, Perpignan, France

Abstract This study was a part of the DeWEX project (**De**ep **W**ater formation **Ex**periment), designed to better understand the impact of dense water formation on the marine biogeochemical cycles. Here, nutrient and phytoplankton vertical and horizontal distributions were investigated during a deep open-ocean convection event and during the following spring bloom in the Northwestern Mediterranean Sea (NWM). In February 2013, the deep convection event established a surface nutrient gradient from the center of the deep convection patch to the surrounding mixed and stratified areas. In the center of the convection area, a slight but significant difference of nitrate, phosphate and silicate concentrations was observed possibly due to the different volume of deep waters included in the mixing or to the sediment resuspension occurring where the mixing reached the bottom. One of this process, or a combination of both, enriched the water column in silicate and phosphate, and altered significantly the stoichiometry in the center of the deep convection area. This alteration favored the local development of microphytoplankton in spring, while nanophytoplankton dominated neighboring locations where the convection reached the deep layer but not the bottom. This study shows that the convection process influences both winter nutrients distribution and spring phytoplankton distribution and community structure. Modifications of the convection's spatial scale and intensity (i.e., convective mixing depth) are likely to have strong consequences on phytoplankton community structure and distribution in the NWM, and thus on the marine food web.

Plain Language Summary The deep open-ocean convection in the Northwestern Mediterranean Sea is an important process for the formation and the circulation of the deep waters of the entire Mediterranean Sea, but also for the local spring phytoplankton bloom. In this study, we showed that variations of the convective mixing depth induced different supply in nitrate, phosphate and silicate, and thus different nutrients ratios in the surface waters. These variations could be the result of pore water release loaded in nutrients because of the sediment resuspension enhanced by the bottom-reached mixing. Because of this phenomenon, the slightly higher silicate concentrations in the center of the convection area favored diatoms development in spring. Modifications of this process because of the climate change could then have some consequences on the phytoplankton community structure and thus on the entire marine food web.

1. Introduction

The Mediterranean Sea is one of the rare regions in the world where deep convection events occur [*Killworth*, 1983]. This process is the primary engine of the thermohaline circulation and is particularly intense in the Gulf of Lions (Northwestern Mediterranean Sea; NWM). Despite a high interannual variability

[*Mermex Group*, 2011; *Herrmann et al*., 2013; *Somot et al*., 2016], a general pattern is observed with two events of convection in midwinter and late winter (see *Houpert et al*. [2016] for details), giving rise to a confined but nonetheless very intense spring bloom [*D'Ortenzio and Ribera d'Alcalà*, 2009]. The productivity of this spring bloom is controlled by the nutrient availability, which in turn depends on the meteorological and the hydrological variabilities [*Gačić et al*., 2002; *Gogou et al*., 2014]. Moreover, some studies showed that some deep convection mixng that reaches the seafloor, induced a resuspension of the sediment [*Martín et al*., 2010; *Stabholz et al*., 2013]. Strong vertical mixing associated with cyclonic submesoscale coherent vortices (SCVs) formed by the deep convection induces an upward diffusion of the resuspended particles. These particles produce a turbidity anomaly that can goes up from the bottom to the surface in about a day [*Durrieu de Madron et al*., 2017]. These cyclonic SCVs, with an averaged time life of a year, preserve the newly formed deep waters in their core, as well as a thick nepheloid layer of 1000–2000 m, and likely spread them throughout the whole NWM basin [*Boss et al*., 2016; *Damien et al*., 2017; this issue]. A stimulation of the deep-sea biological activity was observed, including bioluminescence, thanks to the organic matter supply coming from the erosion of the deep sediment, and also from the surface export during the convective mixing, which is then trapped in the new deep waters [*Tamburini et al*., 2013; *Martini et al*., 2014; *Severin et al*., 2016; *Durrieu de Madron et al*., 2017]. Some impacts on the deep biogeochemical budgets should then be expected.

Several studies showed that the deep convection process is responsible for the introduction of a large amount of nutrients to the surface layer [*Marty and Chiavériny*, 2010; *Estrada et al*., 2014; *Severin et al*., 2014; *Ulses et al*., 2016], which directly influences the intensity of the spring bloom [*Lévy et al*., 1998, 1999; *Taylor and Ferrari*, 2011; *Backhaus et al*., 2003; *Heimbürger et al*., 2013; *Ulses et al*., 2016]. A monitoring of phytoplankton pigments in March 2005 and from mid-March to September 2009 in the NWM revealed the heterogeneity of the spring bloom related to mesoscale processes, and the phytoplankton populations succession from spring (diatoms and haptophyte) to late summer (dinoflagellate and coccolithophores) [*Estrada et al*., 2014]. Another monitoring of the biogeochemistry parameters at DyFAMed enabled the understanding of the seasonal cycles of nutrient and phytoplanktonic groups in the Ligurian Sea [*Marty et al*., 2002]. Nevertheless, the convection area does not always reach the Ligurian Sea. And in most of the studies, the absence of observations during both the deep convection mixing and the following spring bloom periods prevents the establishment of clear correlations between these physical and biological processes.

The sampling difficulties in the open-ocean encourage the use of satellite ocean color remote sensing to first identify chlorophyll patterns and then explain them by known physical and ecological forces [*Longhurst*, 2006]. However, the detailed processes responsible for phytoplankton distribution remain generally unknown due to the lack of in situ observations. *D'Ortenzio and Ribera d'Alcalà* [2009] determined seven bioregions in the entire Mediterranean Sea with one specific region covering the NW Mediterranean basin, characterized by an intense bloom in February to March. This bioregion has recently been divided into two trophic regimes differing in bloom timing and intensity: the "High Bloom" bioregion centered in the deep convection area, and the surrounded "Bloom" bioregion [*Mayot et al*., 2016]. But the heterogeneity of the hydrological structures of the Mediterranean Sea [*Millot*, 1999] and the different light and mixing regimes should produce different subsurface phytoplankton distributions. These subsurface biological patterns are not observable by remote sensing [*Lavigne et al*., 2013; *Mignot et al*., 2014; *Cullen*, 2015], although they contribute significantly to the chlorophyll distribution [*Lavigne et al*., 2015].

Contrary to the well-known general circulation of the NWM [*Béthoux et al*., 1998a; *Send et al*., 1999; *Millot and Taupier-Letage*, 2005], mesoscale hydrological structure locations, frequencies, and dynamic remain misunderstood. These last years, an intensification of the studies of these hydrological structures was done thanks to the development of integrated multiplatforms approaches. The DeWEX project (Deep Water EXperiment) is a multidisciplinary study composed of two main oceanographic cruises conducted during the deep convection event in February 2013 and during the following intense spring bloom in April 2013. Supported by remote sensing and modeling, the DeWEX project aimed to study the hydrological, biogeochemical, and biological processes occurring in the entire NWM basin from the deep convection event in winter to the spring phytoplankton bloom.

In this study, we assessed the impact of the deep convection on the winter nutrients supply, and determined the relative contribution of the resulting nutrient distribution on the phytoplankton distribution and community composition during the spring bloom. Because several stations have similar physicochemical

characteristics, we (i) statistically grouped the winter stations based on their nitrate, phosphate, and silicate concentrations along the water column during the intense convection event of February 2013. Hydrological structures and others physical mechanisms were investigated to understand the distribution of the resulting winter groups. We then (ii) realized a second stations grouping during the spring bloom in April 2013 based on their fluorescence profiles to determine the vertical and horizontal phytoplankton distribution over the NWM. In this section, we also discussed the influence of the winter nutrient supply and intrinsic spring factors on the resulted phytoplankton distribution. Finally, (iii) the resulting winter and spring groups, their nutrients and fluorescence characteristics, and the mechanisms at their origins were used to determine and discuss the spring phytoplankton size class distribution. The occurrence of some phytoplankton groups in specific area was also discussed.

2. Materials and Methods

2.1. Study Area and Sampling

The DeWEX cruises took place in the Northwestern Mediterranean Sea from the 1 to 22 February (Leg 1) and from the 4 to 26 April (Leg 2) 2013 aboard the R/V *Le Suroît*. A network of 76 and 100 stations were prospected during Legs 1 and 2, respectively with a Seabird 911Plus conductivity-temperature-depth (CTD) probe equipped with fluorescence Chelsea Aquatracka III, and an Underwater Vision Profiler (UVP5) [*Picheral et al.*, 2010] providing concentration of large particles (particles L^{-1}) in 27 log-based size classes between 52 μm and 27 mm. At each "biogeochemical" stations (45 during Leg 1, 59 during Leg 2), water samples were collected at 12 levels along the water column with 12 L Niskin bottles mounted on a SBE 32 Carousel water sampler.

2.2. Fluorescence Processing and Calibration

Fluorescence profiles were corrected from the nonphotochemical quenching (NPQ) effect, corrected and adjusted to a zero value at depth and calibrated by leg with the in situ chlorophyll *a* concentrations measured by High Performance Liquid Chromatography (HPLC) according to *Mayot et al.* [2017]. See section 2.3 for pigments analyses.

2.3. Nutrients

Samples for silicate ($Si(OH)_4 \pm 0.05$ μM), nitrate ($NO_3 \pm 0.02$ μM), and phosphate ($PO_4 \pm 0.01$ μM) were immediately stored in 20 ml polyethylene vials at −20°C until analysis. At the laboratory, samples were analyzed by colorimetry on a Seal-Bran-Luebbe autoanalyzer AA3 HR [*Aminot and Kérouel*, 2007].

2.4. Pigments

Pigments samples were collected in 3 L dark bottles, immediately filtered on board through a glass fiber filter (Whatman GF/F 25 mm) sheltered from light and stored in liquid nitrogen until analysis. At the laboratory, pigments were extracted from filters in 100% methanol, disrupted by sonication and clarified by filtration through a glass fiber filter (Whatman GF/F 25 mm). The same day, pigment concentrations were measured by HPLC according to the method proposed by *Ras et al.* [2008]. Pigment analyses were performed at the SAPIGH analytical platform of the Laboratory of Oceanography of Villefranche-sur-mer (CNRS-France).

2.5. Phytoplanktonic Groups

The fractions of chlorophyll *a* (Chl*a*) associated to the three phytoplanktonic groups microphytoplankton, nanophytoplankton, and picophytoplankton were determined from the combination of the concentration of seven key photosynthetic pigments (in μg L^{-1}): fucoxanthin (Fuco), peridinin (Perid), 19′-hexanoyloxyfucaxanthin (Hex), 19′-butanoyloxyfucaxanthin (But), alloxanthin (Allo), chlorophyll *b* + divinyl chlorophyll *b* (TChlb), and zeaxanthin (Zea) according to the equations proposed by *Uitz et al.* [2006]:

$$f_{micro} = \frac{1.41[Fuco] + 1.41[Perid]}{SDP_W}$$

$$f_{nano} = \frac{1.27[Hex - Fuco] + 0.35[But - Fuco] + 0.60[Allo]}{SDP_W}$$

$$f_{pico} = \frac{1.01[TChlb] + 0.86[Zea]}{SDP_W}$$

where:

$$SDP_W = 1.41[Fuco] + 1.41[Perid] + 1.27[Hex-Fuco] + 0.35[But-Fuco] + 0.60[Allo] + 1.01[TChlb] + 0.86[Zea]$$

2.6. Statistical Zonation of the NWM

To understand the impact of the open-ocean convection process on the winter nutrient regime and the spring phytoplankton distribution, we statistically categorized the sampling stations based on their nutrient characteristics in February 2013, and then based on their fluorescence profiles (Chl*a* proxy) in April 2013. Because the deep convection process impacts the entire water column, we chose to take into account both surface and deep biogeochemical properties in February and April to identify the winter nutrients patterns and the variability of the vertical phytoplankton distribution over the NWM. However the interannual variability cannot be assessed by sampling only one month of each key season (February for the winter convection and April for the spring bloom). Therefore, we chose to name the resulting categories "classes" and "subclasses" rather than "bioregions" and "subbioregions," the latter terms being more relevant for a biogeographical study based on several months of observations.

For the winter period, nitrate, phosphate, and silicate surface concentrations, as well as the difference in concentrations between deep (>700 m) and surface (<10 m) layers were selected for the winter NWM zonation in order to take into account the convection effects on the entire water column. For instance, a concentration difference close to zero means that the mixing reached at least the nutricline and enriched the above water column with the nutrients from deep water. For the spring period, we chose the surface fluorescence, the 0–100 m integrated fluorescence, and the depth of the fluorescence maximum as parameters for our statistical analysis. Moreover, the depth of the fluorescence maximum and the 0–100 m integrated fluorescence allowed us to also take into account the phytoplankton distribution in the water column that can vary according to the hydrology and light regime. For this study, we decided to use the fluorescence profiles rather than HPLC data because pigments were analyzed only on 35 out of 100 stations with CTD and fluorescence acquisitions.

Euclidian distances were calculated between the nutrient parameters of the 45 "biogeochemical" stations for the winter period (Leg 1), and then between the fluorescence parameters of the 100 stations for the spring period (Leg 2) using the MATLAB R2015 software. For each period, the resulting Euclidian distances were used to build a hierarchical clustering of the sampling stations using the agglomeration method of Ward. The resulting clusters were named "classes" and "subclasses," as indicated before, and were used to characterize the NWM zonation during the winter and spring 2013.

3. Results

3.1. Winter NWM Zonation and the Associated Hydrology

Three winter classes were distinguished in the NWM from the stations clustering (Leg1 DeWEX, February 2013; Figure 1a; supporting information Figure S1) based on their nutrient characteristics (Figure 2 and Table 1): "*Stratified*," "*Mixed*," and "*Deep Convection*" classes.

The first open-sea class, named "*Stratified*" (14 green stations, Figure 1a), contained stations located on the periphery of the northwestern Mediterranean basin. These stations were marked by a surface layer depleted in nutrient (Figure 2) and a nutricline around 150 m (Table 1). Chl*a* distributions showed inversed patterns compared to nutrients with maximum concentrations in surface layer and generally low concentrations below 150 m. According to the stratified status of these stations, the three NWM water masses were clearly identified along the water column (Figure 3a): Atlantic Waters (AW), Levantine Intermediate Waters (LIW), and Western Mediterranean Deep Waters (WMDW). Two subclasses were identified by hierarchical clustering: "*Stratified 1*" and "*Stratified 2*." The differences were mainly based on the 0–100 m integrated nitrate, phosphate, and silicate concentrations, which were significantly lower (Student test, *p*-value <0.01; Table 1) in the *Stratified 2* subclass (six stations labeled by green circles; Figure 1a) than in the *Stratified 1* subclass (eight stations labeled by green squares; Figure 1a). The subclasses differences were also characterized by significantly higher surface NO_3:PO_4 and $Si(OH)_4$:NO_3 ratios (Student tests, *p*-values <0.001 and <0.01,

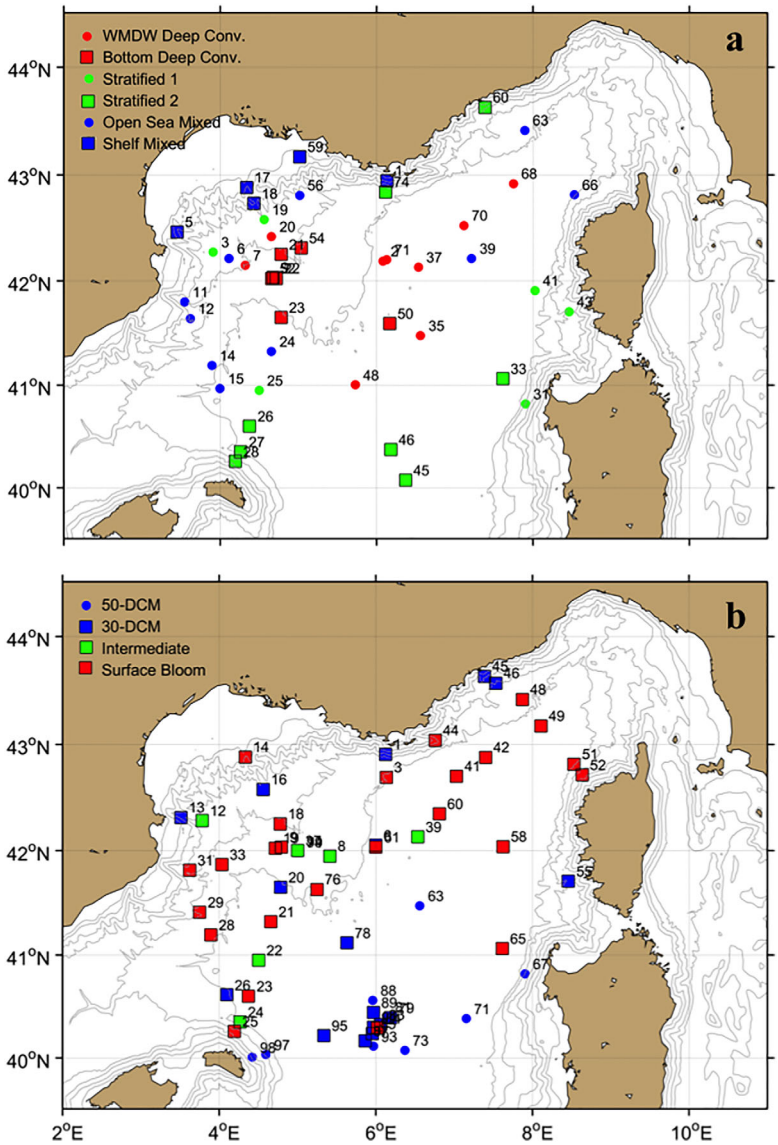

Figure 1. Sampling map during (a) the winter deep convection event (Leg 1 DeWEX cruise, February 2013) and during (b) the spring bloom (Leg 2 DeWEX cruise, April 2013). Colors represent the three classes of each month. (a) Red: *Deep Convection*, blue: *Mixed*, green: *Stratified*; circles are the first subclasses and squares are the seconds (refer to section 3.2 for explanations). (b) Blue: *DCM*, green: *Intermediate*, red: *Surface Bloom*, circles are stations in the *50-DCM* subclass (DCM > 50 m) and squares are the stations in the *30-DCM* subclass (DCM < 30 m) (refer to section 3.3 for explanations).

respectively) in the *Stratified 2* subclass than in the *Stratified 1* subclass (43.66 ± 27.07 and 29.73 ± 3.67, respectively, for NO_3:PO_4 and 1.30 ± 0.32, 0.75 ± 0.08, respectively, for $Si(OH)_4$:NO_3; Table 2).

The second winter class was constituted of stations surrounding the Northern Current (NC) as well as in the Balearic Front (BF) and was named "*Mixed*" according to its hydrological properties described hereafter (15 blue stations, Figure 1a). In general, similar Chl*a* and nutrient profiles were observed in this class compared to the *Stratified* class (Figure 2) with some variations in nutrient concentrations and stoichiometry (Tables 1 and 2). Stations of this *Mixed* class were characterized by mixing of the AW with the upper LIW (Figure 3b), raising the surface layer salinity to 38.11–38.35 (Table 1) compared to the *Stratified* class with a surface salinity range of 38.05–38.25. Nitrate, phosphate, and silicate surface concentrations of the *Mixed* class were significantly higher than in the *Recently Stratified 1* subclass (Student tests, *p*-values <0.01). The hierarchical clustering also resulted in two subclasses distinguished by different locations. The first subclass named "*Open-sea Mixed*" was composed of stations situated offshore (10 stations labeled by blue circles, Figure 1a),

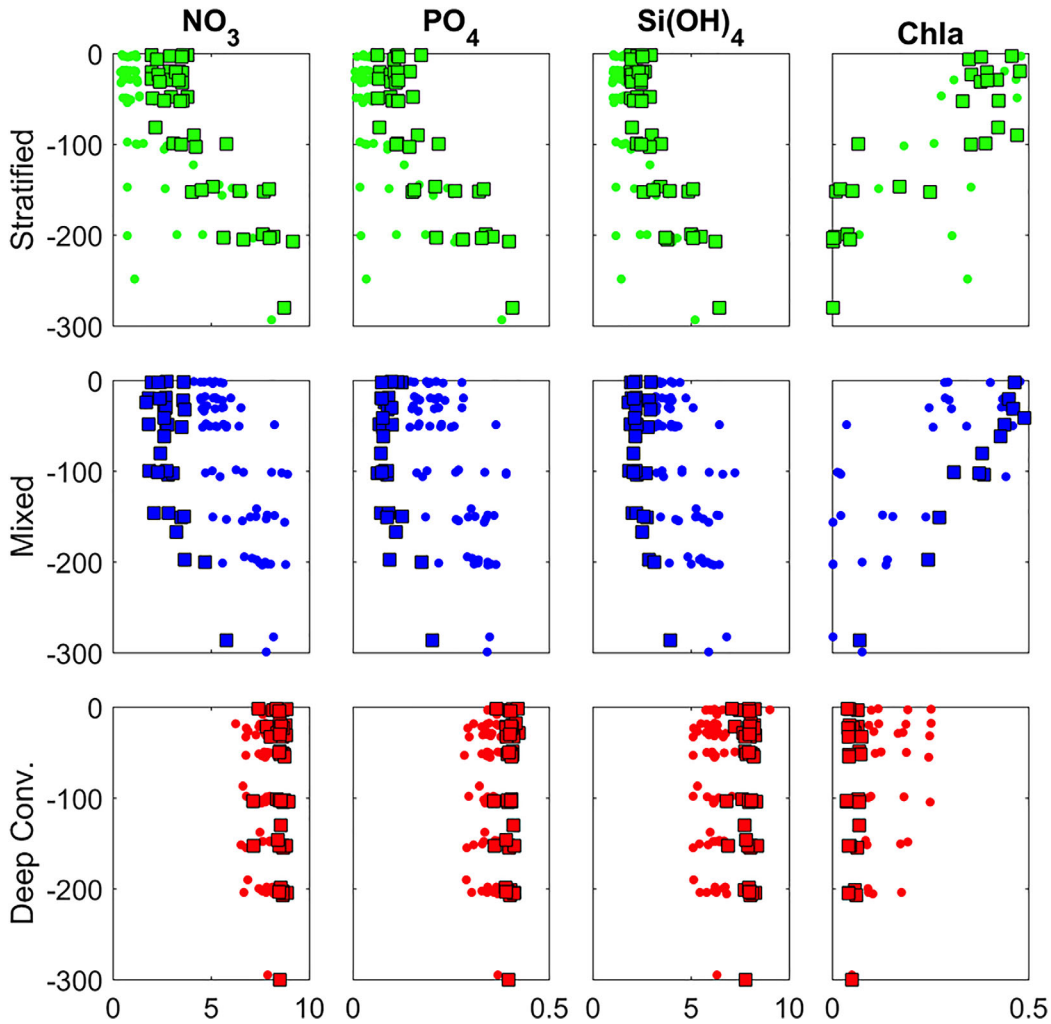

Figure 2. NO_3, PO_4, $Si(OH)_4$ (in µM), and Chl*a* (in µg L^{-1} from HPLC analyses) profiles of each station of the winter class (Leg 1 DeWEX, February 2013). Colors represent the winter classes presented in Figure 1a (red: *Deep Convection*, blue: *Mixed*, green: *Stratified*), circles are the first subclasses and squares the second subclasses.

Table 1. Phosphate (PO_4), Nitrate (NO_3), Silicate ($Si(OH)_4$), and Chlorophyll a (Chl*a*) Mean Concentrations at 10 m and More Than 2000 m (in μM for Nutrient and in μg L^{-1} for Chl*a*) and Mean Integrated (0–100 m) Quantities (in mmol m^{-2} for Nutrient and in mg m^{-2} for Chl*a*), as well as Mean Temperature (T in °C), Salinity (S), and Density Anomaly (d in kg m^{-3}) of Each Winter Class and Subclass of Leg 1[a]

		Stratified		Mixed		Deep Convection	
		1	2	1-Open sea	2-Shelf	1-WMDW	2-Bottom
Surface concentrations (10 m)	NO_3	2.95 ± 0.69	0.82 ± 0.28	5.06 ± 0.45	2.61 ± 0.62	7.64 ± 0.22	8.42 ± 0.34
	PO_4	0.11 ± 0.03	0.03 ± 0.01	0.20 ± 0.03	0.09 ± 0.01	0.35 ± 0.01	0.39 ± 0.01
	$Si(OH)_4$	2.33 ± 0.34	1.34 ± 0.21	3.63 ± 0.49	2.24 ± 0.38	6.32 ± 0.55	7.87 ± 0.30
	Chl*a*	0.45 ± 0.08	0.53 ± 0.08	0.43 ± 0.16	0.53 ± 0.08	0.16 ± 0.07	0.05 ± 0.01
Deep concentrations (>2000 m)	NO_3	8.83 ± 0.25	8.78 ± 0.17	8.70 ± 0.2	NA	8.69 ± 0.10	8.51 ± 0.51
	PO_4	0.41 ± 0.03	0.39 ± 0.00	0.39 ± 0.01	NA	0.40 ± 0.00	0.40 ± 0.01
	$Si(OH)_4$	8.84 ± 0.09	8.79 ± 0.22	8.8 ± 0.17	NA	8.75 ± 0.12	8.32 ± 0.45
Integrated quantities (0–100 m)	NO_3	326 ± 69	127 ± 45	567 ± 97	262 ± 57	758 ± 34	825 ± 64
	PO_4	11.74 ± 2.88	3.97 ± 1.35	22.53 ± 5.77	8.29 ± 0.8	34.1 ± 2.05	38.81 ± 3.25
	$Si(OH)_4$	244 ± 35	151 ± 27	408 ± 90	224 ± 34	611 ± 42	769 ± 64
	Chl*a*	34.23 ± 17.9	15.64 ± 22.1	16.1 ± 20.6	27.7 ± 25.5	7.28 ± 9.56	2.9 ± 2.85
Hydrology (10 m)	T	13.09 ± 0.07	13.51 ± 0.23	13.09 ± 0.12	12.88 ± 0.54	13.09 ± 0.09	12.95 ± 0.02
	S	38.25 ± 0.04	38.05 ± 0.09	38.35 ± 0.09	38.11 ± 0.16	38.50 ± 0.02	38.49 ± 0.005
	d	28.89 ± 0.04	28.65 ± 0.12	28.97 ± 0.08	28.83 ± 0.06	29.09 ± 0.005	29.11 ± 0.004

[a]Standard deviations are indicated after ±. NA for not available data.

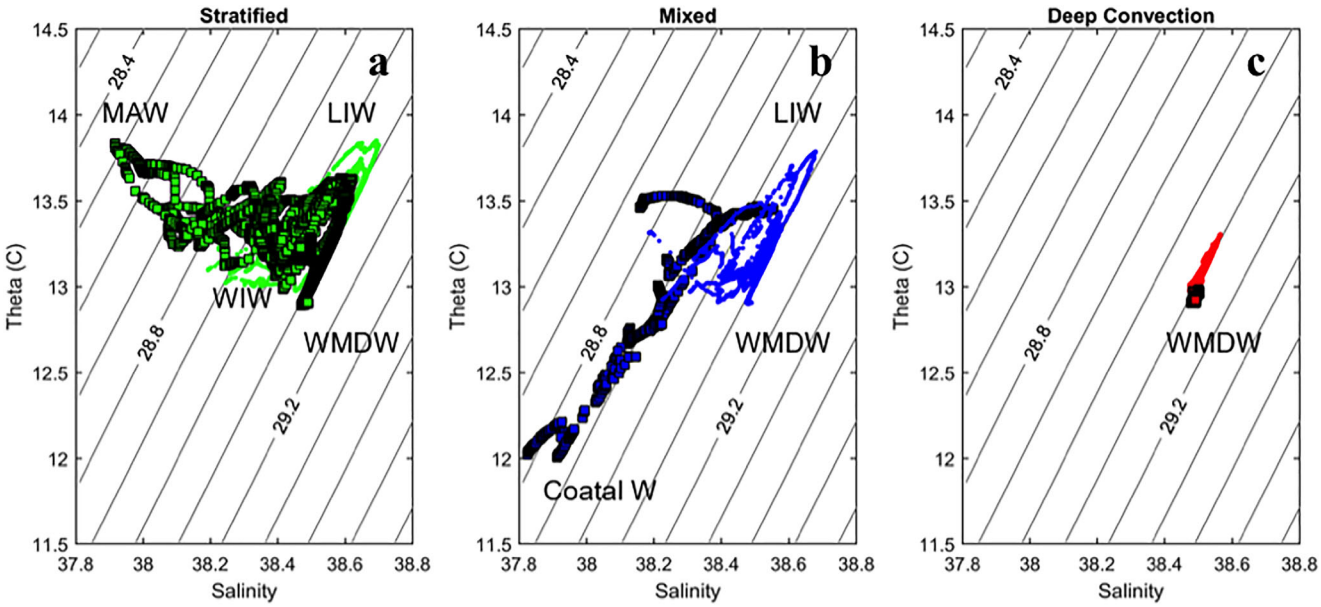

Figure 3. Temperature-salinity diagrams of each stations of the winter classes (Leg 1 DeWEX, February 2013): (a) *Stratified* (in green), (b) *Mixed* (in blue), and (c) *Deep Convection* (in red). Circles are the first subclasses and squares the seconds subclasses presented in Figure 1a.

in contrast to the second subclass "*Shelf Mixed*" (five stations labeled by blue squares, Figure 1a) composed of shallower stations situated on the continental slope marked by the absence of WMDW. These subclasses were characterized by significantly higher surface nutrient concentrations and 0–100 m integrated quantities (Student tests, *p*-values <0.01; Table 1) in the *Open-sea Mixed* subclass compared to the *Shelf Mixed*. Surface $Si(OH)_4$:NO_3 and NO_3:PO_4 ratios were also significantly different (Student tests, *p*-values <0.001 for both) with lower ratios in the *Open-sea Mixed* subclass than in the *Shelf Mixed* ($Si(OH)_4$:$NO_3 = 0.70 \pm 0.04$ and 0.82 ± 0.08 in *Open-sea Mixed* and *Shelf Mixed*, respectively, NO_3:$PO_4 = 26.44 \pm 2.93$ and 32.99 ± 7.55 in *Open-sea Mixed* and *Shelf Mixed*, respectively; Table 2).

The third class named "*Deep Convection*" was constituted of stations situated in the center of the northern gyre of the Gulf of Lions, delimited by the NC and the BF (16 red stations, Figure 1a). This class was characterized by homogeneous nutrient distribution throughout the water column (Table 1 and Figure 2). Consequently, nutrient concentrations in the 0–100 m surface layer were significantly higher in the *Deep Convection* class than in the *Stratified* and *Mixed* classes (Student tests, *p*-values <0.01). Chl*a* concentrations were lower in the surface layer in the *Deep Convection* class compared to the other classes (Figure 2). In contrast to the *Stratified* and *Mixed* classes, Chl*a* was also present below the euphotic zone ($\sim$100 m in winter) with an average concentration of $\sim$0.04 $\mu g\ L^{-1}$ between 500 m and the bottom, while its concentration was null at these depths in the *Stratified* and *Mixed* classes (Figure 2). Only one homogeneous water mass was observed on the Θ/S diagram (Figure 3c and Table 1), characteristic of the convective water mass. Two subclasses were also identified in the *Deep Convection* class. In the first subclass named "*WMDW Deep Convection*" (nine stations labeled by red circles; Figure 1a), nutrient concentrations were slightly but significantly lower (Student tests, *p*-values <0.05) than in the second subclass named "*Bottom Deep Convection*"

Table 2. Mean Nitrate to Phosphate (N:P) and Silicate to Nitrate (Si:N) Ratios Between 0 and 100 m and Deeper Than 700 m of Each Winter Class and Subclass of Leg 1 (Figure 2)[a]

		Stratified		Mixed		Deep Convection	
		1	2	1-Open sea	2-Shelf	1-WMDW	2-Bottom
Mean surface ratio	N:P	29.73 ± 3.67	43.66 ± 27.07	26.44 ± 2.93	32.99 ± 7.55	22.34 ± 0.95	21.22 ± 0.71
(0–100 m)	Si:N	0.75 ± 0.08	1.30 ± 0.32	0.70 ± 0.04	0.82 ± 0.08	0.80 ± 0.06	0.93 ± 0.01
Mean deep ratio	N:P	21.41 ± 0.67	21.53 ± 1.15	21.42 ± 1.30	NA	21.61 ± 0.47	21.29 ± 0.83
(>700 m)	Si:N	1.00 ± 0.03	0.99 ± 0.02	1.00 ± 0.03	NA	0.99 ± 0.04	0.96 ± 0.03

[a]NA for not available data.

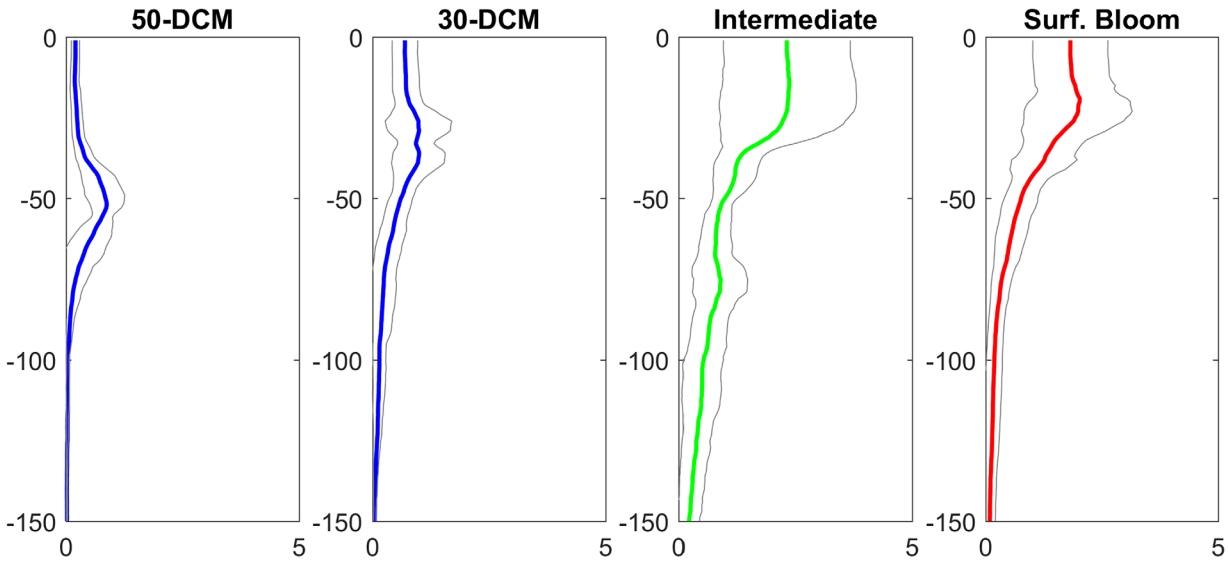

Figure 4. Averaged fluorescence profiles (colored lines) with their standard deviation (grey lines) for each spring class (from left to right): *50-DCM* (blue), *30-DCM* (blue), *Intermediate* (green), and *Surface Bloom* (red) (Leg 2 DeWEX, April 2013).

(seven stations labeled by red squares; Figure 1a). Surface $Si(OH)_4$:NO_3 was slightly but significantly higher (Student test, *p*-value <0.001) in the *Bottom Deep Convection* subclass (0.93 ± 0.01; Table 2) than in the *WMDW Deep Convection* (0.80 ± 0.06; Table 2). In contrast, the NO_3:PO_4 ratios were significantly higher (Student test, *p*-value <0.001) in the *WMDW Deep Convection* subclass (22.34 ± 0.95) than in the *Bottom Deep Convection* subclass (21.22 ± 0.71). Moreover, salinity and temperature of the *WMDW Deep Convection* were slightly higher, with a significant difference for the temperature (Student test, *p*-value <0.05), than those of *Bottom Deep Convection* (38.50 and 38.49, respectively, for the salinity, 13.09°C and 12.05°C, respectively, for the temperature; Figure 3c and Table 1). This was due to the smaller volume of WMDW involved in the mixing at the *WMDW Deep Convection* subclass, which led to a noticeable higher temperature because of the larger LIW contribution compared to the *Bottom Deep Convection* subclass.

3.2. Spring NWM Zonation Based on Vertical Fluorescence Profiles

Three spring classes were distinguished in the NWM from the stations clustering (Leg 2 DeWEX, April 2013; Figure 1b; supporting information Figure S2) based on their fluorescence profiles (Figure 4): "*Surface Bloom*," "*Deep Chlorophyll Maximum*" (*DCM*), and "*Intermediate*" classes. Phytoplankton size class distribution was then determined in each of the spring bloom class (Figure 5).

The first spring class (25 red stations, Figure 1b) was constituted of stations situated in the center of the northern gyre of the Gulf of Lions, where both winter *Deep Convection* and *Mixed* classes were located in February 2013. This

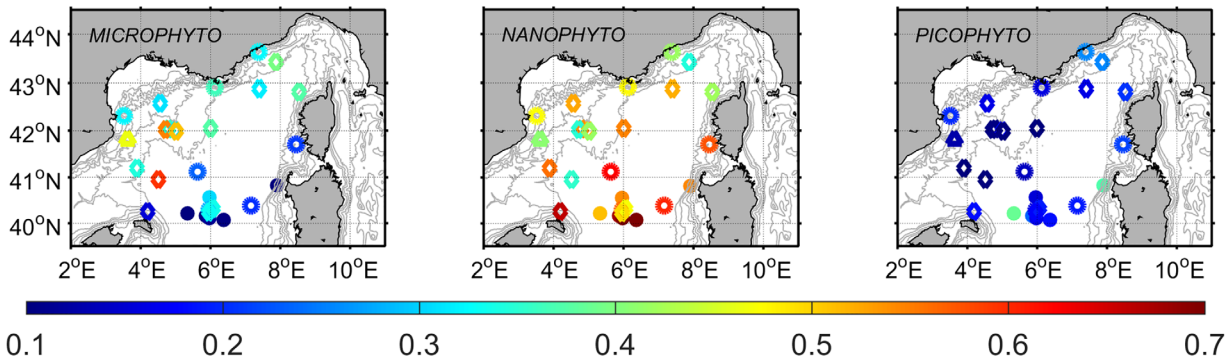

Figure 5. Distribution of the column-integrated fraction of (left) microphytoplankton, (middle) nanophytoplankton, and (right) picophytoplankton with respect to the Chl*a* quantities in spring (Leg 2 DeWEX, April 2013). Shapes represent the spring classes and subclasses presented in Figure 1b: diamonds: *Surface Bloom*, triangles: *Intermediate*, solid circles: *50-DCM*, and empty circles: *30-DCM*.

Table 3. Averages of 0–100 m Integrated Fluorescence (Integrated Fluo. in mgChla m^{-2}), Maximum of Fluorescence (Fluo. max. in mgChl m^{-3}), Depth of the Fluorescence Maximum ($z_{fluo\text{-}max}$ in m), Nitracline (in m), Silicline (in m), Mixed Layer Depth (MLD in m) Calculated With a Potential Density Anomaly Difference of 0.003 kg m^{-3}, and Euphotic Depth (z_e in m) Calculated as the Depth With 1% of the Photosynthetic Active Radiation for Each Spring Class and Subclass of Leg 2[a]

	DCM			
	50-DCM	30-DCM	Intermediate	Surface Bloom
Integrated fluo.	37.49 ± 9.35	66.75 ± 13.26	165.74 ± 25.56	113.21 ± 16.08
Fluo. max.	1.09 ± 0.33	1.26 ± 0.76	2.38 ± 1.44	2.33 ± 1.25
$z_{fluo\text{-}max}$	54 ± 8.03	33.64 ± 11.59	9.83 ± 8.2	20.36 ± 11.16
Nitracline	51.36 ± 19.5	70.29 ± 44.1	50 ± 16.73	55.6 ± 40.7
Silicline	94.54 ± 50.27	87.64 ± 58.15	83.33 ± 38.81	74 ± 39.89
MLD	17.63 ± 10.57	25.94 ± 14.02	30 ± 22.03	22 ± 15.57
z_e	51.78 ± 37.20	25.88 ± 21.74	17.50 ± 15.02	30.29 ± 20.85

[a]Standard deviations are indicated after ±.

centered spring class was named "*Surface Bloom*" according to the shape of the vertical Chl*a* distribution characterized by the absence of a DCM (Figure 4), or more specifically by a shallow maximum of fluorescence (20.36 ± 11.16 m; Table 3). The 0–100 m integrated fluorescence and the maximum of fluorescence (113.21 ± 16.08 mgChl m^{-2} and 2.33 ± 1.25 mgChl m^{-3}, respectively; Table 3) were significantly higher in the *Surface Bloom* class than in the *DCM* class (Student tests, *p*-value <0.001 for both). Microphytoplankton and nanophytoplankton were codominant in the *Surface Bloom* class (Figure 5) with slight differences between the locations. Microphytoplankton was more abundant (60%) than nanophytoplankton (40%) in the center of the Gulf of Lions, where the winter *Bottom Deep Convection* subclass was situated, while in the Ligurian Sea, where both the *WMDW Deep Convection* and the *Open Sea Mixed* subclasses were present, the proportion of nanophytoplankton was higher than the proportion of microphytoplankton (50% and 40%, respectively).

The second spring class (28 blue stations, Figure 1b) named "*Deep Chlorophyll Maximum*" grouped the stations located at the periphery of the *Surface Bloom* class and was characterized by a clear peak of fluorescence deeper than 20 m (Figure 4) and significantly deeper than the *Surface Bloom* class (Student test, *p*-value <0.001). Two subclasses, named *50-DCM* and *30-DCM*, were identified. Their MLD was not significantly different (17.63 ± 10.57 and 25.94 ± 14.02 m for *50-DCM* and *30-DCM*, respectively; Table 3). The subclass *50-DCM* was marked by a significantly deeper DCM (54.00 ± 8.03 m) and a significantly lower 0-100 m integrated fluorescence (37.49 ± 9.35 mgChl m^{-2}) compared to the second subclass (Student tests, *p*-values <0.001) and the *Intermediate* and *Surface Bloom* classes (Student tests on 0–100 m integrated fluorescence, *p*-values <0.001). Stations from *50-DCM* were situated in the southern part of the Gulf of Lions (11 stations labeled by blue circles, Figure 1b). The *30-DCM* subclass had a DCM shallower than 35 m (33.64 ± 11.59 m), with a 0–100 m integrated fluorescence (66.75 ± 13.26 mgChl m^{-2}) also significantly lower than both *Intermediate* and *Surface Bloom* classes (Student tests, *p*-values <0.001 for both). Stations of *30-DCM* subclass (17 stations labeled by blue squares, Figure 1b) were situated in the whole periphery of the northern gyre, but mostly north of the 50-DCM stations. Both subclasses were dominated by nanophytoplankton (~55%; Figure 5), with the copresence of picophytoplankton (~20%) and microphytoplankton (~15%). Some stations situated in the south of the sampling area were characterized by greater proportions of picophytoplankton (~35%) and also a particularly deep DCM (>80 m).

A third spring class (six green stations, Figure 1b) was characterized by a maximum of fluorescence spread over several meters depth from 20 to 60 m (Figure 4). This last spring class, named "*Intermediate*" was only constituted of six stations with high 0–100 m integrated fluorescence (165.74 ± 25.56 mgChl m^{-2}; Table 3), significantly higher than in the *DCM* and *Surface bloom* classes (Student tests, *p*-values <0.001 for both) and was characterized by the dominance of nanophytoplankton (~60%; Figure 5).

4. Discussion

Compared to previous years, the open-ocean deep convection event of February 2013 was particularly intense in terms of duration, spatial extent [*Houpert et al.*, 2016], and of volume of dense water formationed [*Waldman et al.*, 2016]. This event was, therefore, an interesting case to study the influence of the convection process on nutrient dynamics and distribution over the NWM, and its consequences in spring on phytoplankton distribution and community structure.

4.1. Winter Nutrient Distribution Influenced by the Deep Convection Event

During the winter, the nutrient-based clustering resulted in three main classes that distinguish the NWM by a surface nitrate (NO_3), phosphate (PO_4), and silicate ($Si(OH)_4$) concentration gradients from the center of

the *Deep Convection* towards the *Mixed* and *Stratified* surrounding classes (Figure 1 and Table 1). This gradient was similar to the gradient of volume of water mixed by the deep convection event (Figure 3) confirming the strong link between spatial nutrient distribution and the deep convection process. The surface gradient was also discernable in each subclass, even inside the *Deep Convection* class where nutrient concentrations were significantly higher in the *Bottom Deep Convection* subclass than in the *WMDW Deep Convection* subclass (Table 1). This difference could be due to the higher volume of WMDW mixed in the *Bottom Deep Convection* subclass than in the *WMDW Deep Convection* subclass, which could allow introducing more nutrients into the water column from the deep waters. Nevertheless, previous studies in the NWM observed homogeneous nitrate, phosphate, and silicate concentrations in the deep layer, i.e., from 800 m to the bottom [*Béthoux et al*., 1998b; *Pujo-Pay et al*., 2011; *Pasqueron de Fommervault et al*., 2015]. In our study, the mixed layer depth (MLD) reached at least 1000 m in both *WMDW* and *Bottom Deep Convection* subclasses, similar nutrients stoichiometry should thus be observed throughout the water column.

The significantly different $Si(OH)_4$:NO_3 and NO_3:PO_4 in the two *Deep Convection* subclasses (Table 2) might be associated to the sediment resuspension induced by the deep convection event, a process yearly observed in the NWM from 2010 to 2013 [*Durrieu de Madron et al*., 2017]. During this particular event of February 2013, UVP profiles of large particles abundance showed that deep sediment resuspension was triggered only in the *Bottom Deep Convection* subclass, producing a bottom nepheloid layer with a concentration up to 500 particles L^{-1} between 1000 m and the bottom (Figures 6a and 6b). On the contrary, particles concentration in the *WMDW Deep Convection* subclass was significantly lower and homogeneous ($\sim$100 particles L^{-1}) between 500 m and the bottom (Figures 6c and 6d). These observations suggest a water column enrichment of the *Bottom Deep Convection* subclass by pore water release loaded with nutrients, especially silicate [*Durrieu de Madron et al*., 2005]. This process, never observed in open-ocean, is regularly detected in shallow lakes [*Søndergaard et al*., 1992; *Dzialowski et al*., 2008; *Niemistö et al*., 2008] and marine coastal waters [*Mermex Group*, 2011], where sediment resuspension is induced by environmental events such as tidal currents, wind-induced storms [*Fanning et al*., 1982; *Tengberg et al*., 2003; *Garcia-Robledo et al*., 2016] or anthropogenic activities [*Durrieu de Madron et al*., 2005]. Most of these marine studies observed higher nitrate, ammonium and silicate injections than phosphate. But here, the sediment resuspension seemed to preferentially enrich the water column in silicate and phosphate rather than nitrate, as shown by the significantly higher $Si(OH)_4$:NO_3 and lower NO_3:PO_4 ratios in the *Bottom Deep Convection* subclass (Table 2). Nutrients measurements in sediment pore waters during a previous cruise in March 2011 (CASCADE) [*Severin et al*., 2014] showed high concentrations of silicate (47.03 $\pm$ 8.68 μM) and phosphate (0.70 $\pm$ 0.18 μM) compared to nitrate (12.76 $\pm$ 0.81 μM) in the first 2 cm of the sediment cores sampled in the convection area, which resulted in high $Si(OH)_4$:NO_3 (3.71 $\pm$ 0.80) and low NO_3:PO_4 (18.76 $\pm$ 3.13) ratios. These measurements reinforce our hypothesis of a preferential enrichment in silicate and phosphate by sediment resuspension. Moreover, previous studies showed that in oxidized conditions, iron (III) present in the sediment adsorbs phosphorus and favors its sequestration [*Jensen et al*., 1992; *Søndergaard et al*., 2003]. In our study, the strong convective mixing oxidized the whole water column and most probably the surface layer of the sediment, favoring phosphorus adsorption on iron (III). Thus, to observe a phosphate release like in our study, the resuspended sediment should have low iron concentration. To confirm this hypothesis, measurements of phosphate and iron concentrations in the pore water would be required to trace the influence of the sediment resuspension in the water column. Nutrient measurements along the water column prior to a convection event would help to confirm their homogeneity in the deep layer and the inability of different MLD to significantly change the nutrients ratios along the water column.

A previous study on a secondary convection event in the NWM showed that the nutrient supply by a single event was equivalent to the annual supply by the Gulf of Lions rivers, even for an event limited in space (1000 km^2) and time (8 days) during which the MLD only reached the WMDW [*Severin et al*., 2014]. The convection event of March 2011 was preceded by a first deep convection event in February 2011 that reached the bottom. This induced the formation of a bottom nepheloid layer by sediment resuspension that can last almost a year [*Puig et al*., 2013] and was potentially still present during the second convection event sampled in March. This previous mixing event, which reached the bottom, can explain the similar nutrient concentrations and stoichiometry observed in March 2011 and in February 2013, because of either the dilution effect of a higher volume of the WMDW or the pore water release as explain above. Nevertheless, the

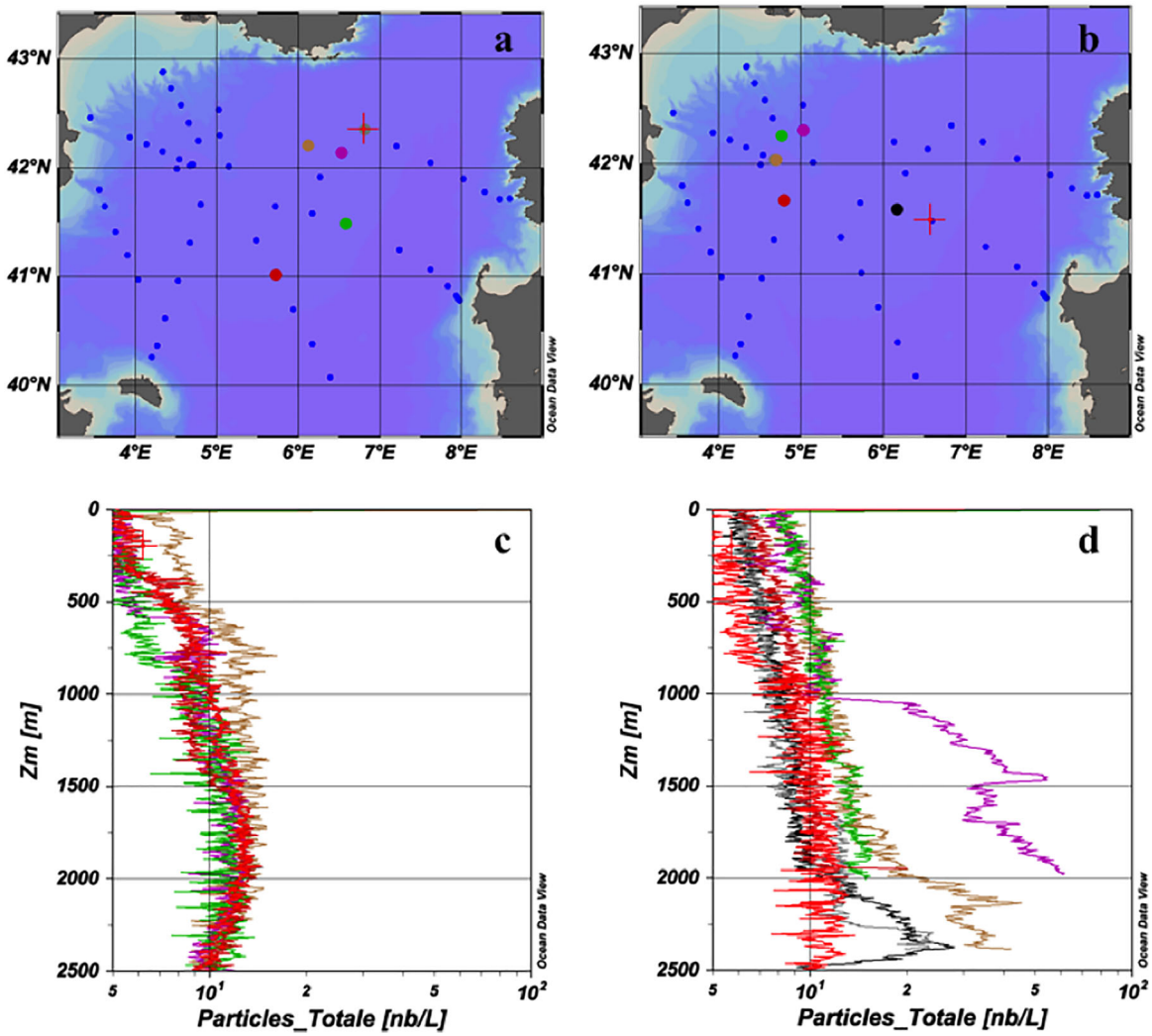

Figure 6. Sampling maps of the winter stations of (a) the *WMDW Deep Convection* and (b) the *Bottom Deep Convection* subclasses, and (c and d) their associated particle concentration profiles (in particles L^{-1}) during the winter deep convection event (Leg 1 DeWEX cruise, February 2013).

convection episode of February 2013 was more extended than the event of March 2011 with an area estimated to 23,600 km^2 [*Houpert et al.*, 2016]. Using the 0–100 m averaged integrated nutrient quantities of the *Deep Convection* class, NO_3, PO_4 and $Si(OH)_4$ supplies were evaluated to $1.87 \pm 0.11 \times 10^{10}$, $8.60 \pm 0.78 \times 10^8$, and $1.63 \pm 0.26 \times 10^{10}$ mol, respectively, so 23 times more nutrients than in March 2011 and only 1.5 times more than in February 2011 [*Severin et al.*, 2014]. Using physical/biogeochemical coupled modeling, *Ulses et al.* [2016] estimated supplies of nutrients at 100 m depth in the NWM. They obtained 5 times more than our estimates for the strongly convective winter 2004–2005, and 2.5 and 1.7 more than our estimates for the less convective winters, respectively, 2005–2006 and 2003–2004 winters. Unfortunately, these studies used different criteria to delimit the convection area, which lead to significant variations in the nutrient supplies estimates [*Houpert et al.*, 2016]. This can cause an over or underestimation of the nutrients budgets, which highlights the necessity to choose a unique criterion to determine the convection area.

4.2. Spring Phytoplankton Abundance and Horizontal Distribution Influenced by Winter Nutrients Supply

In spring, the superposition of the fluorescence-based classes with the winter nutrient-based classes (Figure 1) confirmed the previous observations that the winter nutrient supply by the convection process is one the main factors influencing the spring phytoplankton bloom [*Lévy et al.*, 1998; *Gačić et al.*, 2002; *Heimbürger et al.*, 2013]. Indeed, the fluorescence characteristics (Table 3) indicated that the phytoplankton bloom was centered

in the northern cyclonic gyre of the NWM, i.e., in the *Surface Bloom* class which corresponded to the winter *Open Sea Mixed* and *Deep Convection* classes (Figure 1). Consequently, the convection process controls the winter nutrient supply (Table 1), which in turn influences the phytoplankton surface abundance and horizontal distribution in spring. The predicted decrease in intensity and coverage of the convection process with climate change [*Giorgi*, 2006; *Somot et al*., 2006] could, therefore, have consequences on the phytoplankton ecosystem, as already observed in some predictive models [*Herrmann et al*., 2014; *Macias et al*., 2015].

But while the large winter nutrient supply induced a bloom with a surface fluorescence maximum (Figure 4 and Table 3), the phytoplankton vertical distribution in the surrounding *DCM* and *Intermediate* classes cannot be explain by the deep convection process. Because the *DCM* class was located where the winter *Stratified* class was, the nutrient-depleted surface layer certainly favored a deep phytoplankton development closer to the nutricline (Table 3), and thus the formation of a DCM. Moreover, the significant correlation between the MLD and the depth of the fluorescence maximum (Spearman test, $r = -0.322$, p-value <0.05; supporting information Table S1) indicated that MLD variations could be responsible for the different DCM observed (*50-DCM* versus *30-DCM* subclasses), as well as some station mismatches between the winter and spring classes (Figure 1). For instance, spring stations 23 and 25 and the southern stations 83 and 85 did not benefit from the winter nutrient supply, but a short MLD deepening prior the sampling enable a surface phytoplankton development characteristic of the *Surface Bloom* class (Figure 4 and Table 3). Inversely, the spring station 78 was in the winter *Deep Convection* class, but an early MLD shallowing in spring resulted in a low and deep fluorescence maximum, characteristic for a *DCM* class (Figure 4 and Table 3). Thus, in nutrient-depleted waters, a shallow MLD induces a deep DCM and reciprocally. In our study, the phytoplankton distribution was evaluated via fluorescence measurements, the observed DCMs could thus be a consequence of photoacclimation processes and not an actual deep phytoplankton biomass maximum. In this case, the maximum of fluorescence should increase with the deepening of the DCM. Here the maximum of fluorescence was significantly lower in the *50-DCM* than in the *30-DCM* subclasses (Table 3), which suggests that the DCM was associated with a biomass maximum. Counting of phytoplankton cells throughout the water column would be necessary to confirm this hypothesis.

Several studies showed the influence of the MLD on the phytoplankton vertical distribution, in association with others biotic and abiotic mechanisms such as the light regime, predations, or phytoplankton growth and sinking [*Morel and Berthon*, 1989; *Estrada et al*., 1993; *Mignot et al*., 2014; *Lavigne et al*., 2015; *Cullen*, 2015, and references therein]. Unfortunately, the resolution of our study with sampling once per month in February and April prevents to identify these other mechanisms, as shown by the absence of correlation between the fluorescence maximum depth and the euphotic depth or the nutriclines (supporting information Table S1). Nevertheless, a study showed that the duration and depth of the convective mixing directly shape both the phenology and the magnitude of the spring bloom in the NWM [*Lavigne et al*., 2013]. Moreover, a 1 year study covering the 2013 deep convection event and spring bloom [*Mayot et al*., 2017] confirmed this hypothesis, which strengthens our study which uses data from the convection event in February to explain the phytoplankton distribution in April. In this study, they observed two bioregions similar to our *Surface Bloom* and *DCM* classes with a significant higher phytoplankton accumulation in the former class similar to our study. Similarly, they explained this difference by higher silicate availability and a reduced zooplankton grazing pressure because of a greater dilution by the convective mixing [*Behrenfeld*, 2010].

4.3. Winter Nutrient Supply Induced the Spring Phytoplankton Size Class Distribution

Several studies showed clear correlations between phytoplankton size classes and nutrient stocks and stoichiometry [*Staehr et al*., 2002; *Elser et al*., 2003; *Conan et al*., 2007; *Meyer et al*., 2016]. The *Surface Bloom* class, characterized by the highest winter nutrient replenishment in our study, was codominated by microphytoplankton and nanophytoplankton as expected (i.e., larger cells), while nanophytoplankton and picophytoplankton dominated the *DCM* class (Figure 5).

In this classical general scheme, another pattern was observable when considering the spring proportion of microphytoplankton and nanophytoplankton in the winter classes. Within the *Surface Bloom* class, microphytoplankton was dominant where the winter *Bottom Deep Convection* subclass was located, while nanophytoplankton dominated the *WMDW Deep Convection* and the *Open-Sea Mixed* subclasses. To explain such a difference, it is necessary to consider the winter nutrient stoichiometry (Table 2). Microphytoplankton was

clearly related to elevated winter concentrations of NO_3, PO_4, and $Si(OH)_4$, but also with relatively low NO_3:PO_4 and high $Si(OH)_4$:NO_3 ratios. In our study, microphytoplankton group was defined using fucoxanthin and peridinin, characteristic pigments of diatoms and dinoflagellates, respectively [*Uitz et al*., 2006]. Diatoms are known to be opportunist and to grow in enriched environments with relatively low $Si(OH)_4$:NO_3:PO_4 ratios [*Conan et al*., 2007]. The large silicate supply in the *Bottom Deep Convection* subclass, evidenced by the high $Si(OH)_4$:NO_3, seemed to favor diatoms rather than dinoflagellates. This was confirmed by the 0–100 m integrated fucoxanthin to peridinin proportion index (Fucoxanthin/[Fucoxanthin + Peridinin]) that was higher in the *Surface Bloom* stations previously located in the *Bottom Deep Convection* subclass (99.81 ± 2.74) than in the *WMDW Deep Convection* and *Open-Sea Mixed* subclasses (86.16 ± 7.60). The only exceptions were the previously mentioned spring stations 23 and 25 (Figure 1b) dominated by microphytoplankton and nanophytoplankton, respectively (Figure 5) and the southern stations 83 and 85 also (Figure 1b) dominated by nanophytoplankton (Figure 5), although they were located in the nutrient-depleted winter *Stratified* class. The short MLD deepening enriched these stations enough to have a similar phytoplankton development than the nutrient-enriched *Deep Convection* and *Mixed* classes. Nevertheless the large size range of the diatoms, from nanosized to microsized classes, is not taken into account with the method used in our study to determine the phytoplankton community structure [*Uitz et al*., 2006]. While previous studies in the NWM observed diatoms bloom of the microphytoplankton size class [*Percopo et al*., 2011; *Rigual-Hernández et al*., 2013], it is possible that smaller diatoms taxa become dominant like in the North Atlantic spring bloom because of changes in the environmental conditions [*Daniels et al*., 2015].

Concerning the nanophytoplankton and picophytoplankton that dominated the *DCM* class, the nutrient-depleted surface layer and the high NO_3:PO_4 and low $Si(OH)_4$:NO_3 ratios (Tables 1 and 2) combined to favor smaller cells development [*Pujo-Pay et al*., 2011]. Moreover, picophytoplankton was more abundant in the southern stations of the *50-DCM* subclass, where the winter *Stratified 2* subclass occurred (Figure 1b) characterized by the lower surface nutrient concentrations and the highest surface NO_3:PO_4 and $Si(OH)_4$:NO_3 ratios (Table 2). These nutrient stocks, in association with the significantly deeper euphotic depth in the *50-DCM* than in the *30-DCM* subclasses (Table 3; Student test, p-value = 0.041), created the ideal conditions to promote the picophytoplankton development more adapted to oligotrophic waters [*Clark et al*., 2013]. Finally, the presence of some microphytoplankton in the northern stations from the *30-DCM* subclass (~30%; Figures 1b and 5) could be due to a nutrient enrichment by the rivers' discharge. Even if the annual nutrient supply by the rivers is significantly lower than the supply by a single convection event [*Severin et al*., 2014], this input in coastal waters was enough to favor a microphytoplankton development.

5. Conclusion

In this study, we showed that the spatial extent of the deep convection process directly determines silicate, nitrate, and phosphate concentrations over the NWM, while the convective mixing depth conditions the nutrient stoichiometry by dilution effect of the WMDW or because of the sediment resuspension triggered by bottom reaching mixing. In turn, the winter nutrient supply influences the spring phytoplankton abundance and horizontal distribution, while the winter nutrient stoichiometry impacts the spring phytoplankton community structure, favoring diatoms in the center of the deep convection area enriched in silicate.

The expected changes of the convection process due to climate change will have consequences for phytoplankton abundance and community structure in spring. Reduced convection events in time, space, and in mixing depth, like in 2008, will diminish the nutrient supplies, especially in silicate. This can lead to an ecosystem shift by favoring dinoflagellates, or picophytoplankton, if the deep convection process completely disappears, with consequences for biogeochemical cycles and on the entire marine food web.

Acknowledgments
We are grateful to the crew and officials of R/V *Le Suroit* and to all the scientific and technical staff involved in the DeWEX cruise for their support during sea operations. This study was supported by the programs MOOSE, MerMex, and HyMeX projects under the MISTRALS framework. Data used in this study are referenced by SISMER (https://doi.org/10.17600/13020010; https://doi.org/10.17600/13020030).

References

Aminot, A., and R. Kérouel (2007), *Dosage Automatique des Nutriments Dans les Eaux Marines: Méthodes en Flux Continu*., Ifremer, Brest.
Backhaus, J. O., E. N. Hegseth, X. Irigoien, K. Hatten, and K. Logemann (2003), Convection and primary production in winter, *Mar. Ecol. Prog. Ser*., *251*, 1–14.
Behrenfeld, M. J. (2010), Abandoning Sverdrup's critical depth hypothesis on phytoplankton blooms, *Ecology*, *91*(4), 977–989, doi:10.1890/09-1207.1.

Béthoux, J. P., B. Gentili, and D. Tailliez (1998a), Warming and freshwater budget change in the Mediterranean since the 1940s, their possible relation to the greenhouse effect, *Geophys. Res. Lett.*, *25*, 1023–1026.
Béthoux, J. P., P. Morin, C. Chaumery, O. Connan, B. Gentili, and D. Ruiz-Pino (1998b), Nutrients in the Mediterranean Sea, mass balance and statistical analysis of concentrations with respect to environmental change, *Mar. Chem.*, *63*, 155–169.
Boss, A., et al. (2016), Scales and dynamics of submesoscale coherent vortices formed by deep convection in the northwestern Mediterranean sea. *J. Geophys. Res. Oceans.*, *121*, 7716–7742. doi:10.1002/2016JC012144.
Clark, J. R., T. M. Lenton, H. T. P. Williams, and S. J. Daine (2013), Environmental selection resource allocation determine spatial patterns in picophytoplankton cell size, *Limnol. Oceanogr. Methods*, *58*(3), 1008–1022, doi:10.4319/lo.2013.58.3.1008.
Conan, P., M. Søndergaard, T. Kragh, F. Thingstad, M. Pujo-Pay, P. J. L. B. Williams, S. Markager, G. Cauwet, N. H. Borch, and D. Evans (2007), Partitioning of organic production in marine plankton communities: The effects of inorganic nutrient ratios and community composition on new dissolved organic matter, *Limnol. Oceanogr. Methods*, *52*(2), 753–765, doi:10.4319/lo.2007.52.2.0753.
Cullen, J. J. (2015), Subsurface chlorophyll maximum layers: enduring enigma or mystery solved? *Annu. Rev. Mar. Sci.*, *7*, 207–239, doi: 10.1146/annurev-marine-010213-135111.
Damien P., A. Bosse, P. Testor, P. Marsaleix, and C. Estournel (2017), Modeling postconvective submesoscale coherent vortices in the northwestern Mediterranean Sea, *J. Geophys. Res. Oceans*, *122*, doi:10.1002/2016JC012114.
Daniels, C. J., A. J. Poulton, M. Esposito, M. L. Paulsen, R. Bellerby, M. St John, and A. P. Martin (2015), Phytoplankton dynamics in contrasting early stage North Atlantic spring blooms: Composition, succession, and potential drivers, *Biogeosciences*, *12*(8), 2395–2409, doi: 10.5194/bg-12-2395-2015.
D'Ortenzio, F., and M. Ribera d'Alcalà (2009), On the trophic regimes of the Mediterranean Sea: A satellite analysis, *Biogeosciences*, *6*, 1–10.
Durrieu de Madron, X., B. Ferré, G. Le Corre, C. Grenz, P. Conan, M. Pujo-Pay, R. Buscail, and O. Bodiot (2005), Trawling-induced resuspension and dispersal of muddy sediments and dissolved elements in the Gulf of Lion (NW Mediterranean), *Cont. Shelf Res.*, *25*(19–20), 2387–2409, doi:10.1016/j.csr.2005.08.002.
Durrieu de Madron, X., et al. (2017), Deep sediment resuspension and thick nepheloid layer generation by open-ocean convection, *J. Geophys. Res. Oceans*, *122*, 2291–2318, doi:10.1002/2016JC012062.
Dzialowski, A. R., S. Wang, N. Lim, J. H. Beury, and D. G. Huggins (2008), Effects of sediment resuspension on nutrient concentrations and algal biomass in reservoirs of the Central Plains, *Lake Reserv. Manage.*, *24*(4), 313–320, doi:10.1080/07438140809354841.
Elser, J. J., M. Kyle, W. Makino, T. Yoshida, and J. Urabe (2003), Ecological stoichiometry in the microbial food web: A test of the light:nutrient hypothesis, *Aquat. Microb. Ecol.*, *31(1)*, 49–65, doi:10.3354/ame031049.
Estrada, M., C. Marrasé, M. Latasa, E. Berdalet, M. Delgado, and T. Riera (1993), Variability of deep chlorophyll maximum characteristics in the Northwestern Mediterranean, *Mar. Ecol. Prog. Ser.*, *92*, 289–300.
Estrada, M., M. Latasa, M. Emelianov, A. Gutiérrez-Rodríguez, B. Fernández-Castro, J. Isern-Fontanet, B. Mouriño-Carballido, J. Salat, and M. Vidal (2014), Seasonal and mesoscale variability of primary production in the deep winter-mixing region of the NW Mediterranean, *Deep Sea Res., Part I*, *94*, 45–61, doi:10.1016/j.dsr.2014.08.003.
Fanning, K. A., K. L. Carder, and P. R. Betzer (1982), Sediment resuspension by coastal waters: A potential mechanism for nutrient re-cycling on the Ocean's margins, *Deep Sea Res., Part A*, *29*(8), 953–965, doi:10.1016/0198-0149(82)90020-6.
Gačić, M., G. Civitarese, S. Miserocchi, V. Cardin, A. Crise, and E. Mauri (2002), The open-ocean convection in the Southern Adriatic: A controlling mechanism of the spring phytoplankton bloom, *Cont. Shelf Res.*, *22*, 1897–1908, doi:10.1016/S0278-4343(02)00050-X.
Garcia-Robledo, E., J. Bohorquez, A. Corzo, J. L. Jimenez-Arias, and S. Papaspyrou (2016), Dynamics of inorganic nutrients in intertidal sediments: Porewater, exchangeable, and intracellular pools, *Front. Microbiol.*, *7*, 761, doi:10.3389/fmicb.2016.00761.
Giorgi, F. (2006), Climate change hot-spots, *Geophys. Res. Lett.*, *33*, L08707, doi:10.1029/2006GL025734.
Gogou, A., et al. (2014), Carbon flux to the deep in three open sites of the Southern European Seas (SES), *J. Mar. Syst.*, *129*, 224–233, doi: 10.1016/j.jmarsys.2013.05.013.
Heimbürger, L.-E., H. Lavigne, C. Migon, F. D'Ortenzio, C. Estournel, L. Coppola, and J.-C. Miquel (2013), Temporal variability of vertical export flux at the DYFAMED time-series station (Northwestern Mediterranean Sea), *Prog. Oceanogr.*, *119*, 59–67, doi:10.1016/j.pocean.2013.08.005.
Herrmann, M., F. Diaz, C. Estournel, P. Marsaleix, and C. Ulses (2013), Impact of atmospheric and oceanic interannual variability on the Northwestern Mediterranean Sea pelagic planktonic ecosystem and associated carbon cycle, *J. Geophys. Res. Oceans*, *118*, 5792–5813, doi:10.1002/jgrc.20405.
Herrmann, M., C. Estournel, F. Adloff, and F. Diaz (2014), Impact of climate change on the northwestern Mediterranean Sea pelagic planktonic ecosystem and associated carbon cycle, *J. Geophys. Res. Oceans*, *119*, 5815–5836, doi:10.1002/2014JC010016.
Houpert, L., et al. (2016), Observations of open-ocean deep convection in the northwestern Mediterranean Sea: Seasonal and interannual variability of mixing and deep water masses for the 2007–2013 period, *J. Geophys. Res. Oceans*, *121*, 8139–8171, doi:10.1002/2016JC011857.
Jensen, H. S., P. Kristensen, E. Jeppesen, and A. Skytthe (1992), Iron-phosphorus ratio in surface sediment as an indicator of phosphate release from aerobic sediments in shallow lakes, *Hydrobiologia*, *235/236*, 731–743.
Killworth, P. D. (1983), Deep convection in the World Ocean, *Rev. Geophys.*, *21*, 1–26, doi:10.1029/RG021i001p00001.
Lavigne, H., F. D'Ortenzio, C. Migon, H. Claustre, P. Testor, M. R. D'Alcalà, R. Lavezza, L. Houpert, and L. Prieur (2013), Enhancing the comprehension of mixed layer depth control on the Mediterranean phytoplankton phenology, *J. Geophys. Res. Oceans*, *118*, 3416–3430, doi:10.1002/jgrc.20251.
Lavigne, H., F. D'Ortenzio, M. Ribera D'Alcalà, H. Claustre, R. Sauzède, and M. Gacic (2015), On the vertical distribution of the chlorophyll a concentration in the Mediterranean Sea: A basin scale and seasonal approach, *Biogeosciences*, *12*, 5021–5039, doi:10.5194/bg-12-5021-2015.
Lévy, M., L. Memery, and G. Madec (1998), The onset of a bloom after deep winter convection in the northwestern Mediterranean sea: Mesoscale process study with a primitive equation model, *J. Mar. Syst.*, *16*, 7–21.
Lévy, M., L. Mémery, and G. Madec (1999), The onset of the spring bloom in the MEDOC area: Mesoscale spatial variability, *Deep Sea Res., Part I*, *46*, 1137–1160.
Longhurst, A. R. (2006), *Ecological Geography of the Sea*, 2nd ed., Academic press, Burlington.
Macias, D. M., E. Garcia-Gorriz, and A. Stips (2015), Productivity changes in the Mediterranean Sea for the twenty-first century in response to changes in the regional atmospheric forcing, *Front. Mar. Sci.*, *2*(79), 1–13, doi:10.3389/fmars.2015.00079.
Martín, J., J.-C. Miquel, and A. Khripounoff (2010), Impact of open sea deep convection on sediment remobilization in the western Mediterranean, *Geophys. Res. Lett.*, *37*, L13604, doi:10.1029/2010GL043704.
Martini, S., D. Nerini, and C. Tamburini (2014), Relation between deep bioluminescence and oceanographic variables: A statistical analysis using time–frequency decompositions, *Prog. Oceanogr.*, *127*, 117–128.
Marty, J., J. Chiavérini, M. Pizay, and B. Avril (2002), Seasonal and interannual dynamics of nutrients and phytoplankton pigments in the western Mediterranean Sea at the DYFAMED time-series station (1991–1999), *Deep Sea Res., Part II*, *49*, 1965–1985.

Marty, J. C. and J. Chiavéini (2010), Hydrological changes in the Ligurian Sea (NW Mediterranean, DYFAMED site) during 1995–2007 and biogeochemical consequences, *Biogeosci. Discuss.*, *7*(1), 1377–1406, doi:10.5194/bgd-7-1377-2010.

Mayot, N., F. D'Ortenzio, M. Ribera d'Alcalà, H. Lavigne, and H. Claustre (2016), Interannual variability of the Mediterranean trophic regimes from ocean color satellites, *Biogeosciences*, *13*, 1901–1917, doi:10.5194/bg-13-1901-2016.

Mayot, N., F. D'Ortenzio, V. Taillandier, L. Prieur, O. Pasqueron de Fommervault, H. Claustre, A. Bosse, P. Testor, and P. Conan (2017), Physical and biogeochemical controls of the phytoplankton blooms in North-Western Mediterranean Sea: A multiplatform approach over a complete annual cycle (2012–2013 DEWEX experiment), *J. Geophys. Res. Oceans*, doi:10.1002/2016JC012052, in press.

Mermex Group (2011), Marine ecosystems' responses to climatic and anthropogenic forcings in the Mediterranean, *Prog. Oceanogr.*, *91*(2), 97–166, doi:10.1016/j.pocean.2011.02.003.

Meyer, J., C. R. Löscher, S. C. Neulinger, A. F. Reichel, A. Loginova, C. Borchard, R. A. Schmitz, H. Hauss, R. Kiko, and U. Riebesell (2016), Changing nutrient stoichiometry affects phytoplankton production, DOP accumulation and dinitrogen fixation—A mesocosm experiment in the eastern tropical North Atlantic, *Biogeosciences*, *13*(3), 781–794, doi:10.5194/bg-13-781-2016.

Mignot, A., H. Claustre, J. Uitz, A. Poteau, F. D'Ortenzio, and X. Xing (2014), Understanding the seasonal dynamics of phytoplankton biomass and the deep chlorophyll maximum in oligotrophic environments: A Bio-Argo float investigation, *Global Biogeochem. Cycles*, *28*, 856–876, doi:10.1002/2013GB004781.

Millot, C. (1999), Circulation in the Western Mediterranean Sea, *J. Mar. Syst.*, *20*(1–4), 423–442, doi:10.1016/S0924-7963(98)00078-5.

Millot, C., and I. Taupier-Letage (2005), Circulation in the Mediterranean Sea, in *The Mediterranean Sea*, edited by A. Saliot, pp. 29–66, Springer, Berlin.

Morel, A., and J.-F. Berthon (1989), Surface pigments, algal biomass profiles, and potential production of the euphotic layer: Relationships reinvestigated in view of remote-sensing applications, *Limnol. Oceanogr.*, *34*(8), 1545–1562, doi:10.4319/lo.1989.34.8.1545.

Niemistö, J., H. Holmroos, Z. Pekcan-Hekim, and J. Horppila (2008), Interactions between sediment resuspension and sediment quality decrease the TN:TP ratio in a shallow lake, *Limnol. Oceanogr. Methods*, *53*(6), 2407–2415, doi:10.2307/40058331.

Pasqueron de Fommervault, O., C. Migon, F. D'Ortenzio, M. Ribera d'Alcalà, and L. Coppola (2015), Temporal variability of nutrient concentrations in the northwestern Mediterranean sea (DYFAMED time-series station), *Deep Sea Res., Part I*, *100*, 1–12, doi:10.1016/j.dsr.2015.02.006.

Percopo, I., R. Siano, F. Cerino, D. Sarno, and A. Zingone (2011), Phytoplankton diversity during the spring bloom in the northwestern Mediterranean Sea, *Bot. Mar.*, *54*(3), 243–267, doi:10.1515/BOT.2011.033.

Picheral M., L. Guidi, L. Stemmann, D. M. Karl, G. Iddaoud, and G. Gorsky (2010), The Underwater Vision Profiler 5: An advanced instrument for high spatial resolution studies of particle size spectra and zooplankton, *Limnol. Oceanogr. Methods*, *8*, 462–473.

Puig, P., et al. (2013), Thick bottom nepheloid layers in the western Mediterranean generated by deep dense shelf water cascading, *Prog. Oceanogr.*, *111*, 1–23, doi:10.1016/j.pocean.2012.10.003.

Pujo-Pay, M., P. Conan, L. Oriol, V. Cornet-Barthaux, C. Falco, J.-F. Ghiglione, C. Goyet, T. Moutin, and L. Prieur (2011), Integrated survey of elemental stoichiometry (C, N, P) from the western to eastern Mediterranean Sea, *Biogeosciences*, *8*(4), 883–899, doi:10.5194/bg-8-883-2011.

Ras, J., J. Uitz, and H. Claustre (2008), Spatial variability of phytoplankton pigment distributions in the Subtropical South Pacific Ocean: Comparison between in situ and modelled data, *Biogeosciences*, *5*, 353–369.

Rigual-Hernández, A. S., M. A. Bárcena, R. W. Jordan, F. J. Sierro, J. A. Flores, K. J. S. Meier, L. Beaufort, and S. Heussner (2013), Diatom fluxes in the NW Mediterranean: Evidence from a 12-year sediment trap record and surficial sediments, *J. Plankton Res.*, *35*(5), 1109–1125, doi:10.1093/plankt/fbt055.

Send, U., J. Font, G. Krahmann, C. Millot, M. Rhein, and J. Tintoré (1999), Recent advances in observing the physical oceanography of the western Mediterranean Sea, *Prog. Oceanogr.*, *44*, 37–64, doi:10.1016/S0079-6611(99)00020-8.

Severin, T., P. Conan, X. Durrieu de Madron, L. Houpert, M. J. Oliver, L. Oriol, J. Caparros, J. F. Ghiglione, and M. Pujo-Pay (2014), Impact of open-ocean convection on nutrients, phytoplankton biomass and activity, *Deep Sea Res., Part I*, *94*, 62–71, doi:10.1016/j.dsr.2014.07.015.

Severin, T., et al. (2016), Impact of an intense water column mixing (0–1500 m) on prokaryotic diversity and activities during an open-ocean convection event in the NW Mediterranean Sea, *Environ. Microbiol.*, *18*, 4378–4390, doi:10.1111/1462-2920.13324.

Somot, S., F. Sevault, and D. Michel (2006), Transient climate change scenario simulation of the Mediterranean Sea for the 21st century using a high-resolution ocean circulation model, *Clim. Dyn.*, *27*(7–8), 851–879.

Somot, S., et al. (2016), Characterizing, modelling and understanding the climate variability of the deep water formation in the North-Western Mediterranean Sea, *Clim. Dyn.*, doi:10.1007/s00382-016-3295-0.

Søndergaard, M., P. Kristensen, and E. Jeppesen (1992), Phosphorus release from resuspended sediment in the shallow and wind-exposed Lake Arresø, Denmark, *Hydrobiologia*, *228*(1), 91–99, doi:10.1007/BF00006480.

Søndergaard, M., J. P. Jensen, and E. Jeppesen (2003), Role of sediment and internal loading of phosphorus in shallow lakes, *Hydrobiologia*, *506–509*, 135–145.

Stabholz, M., et al. (2013), Impact of open-ocean convection on particle fluxes and sediment dynamics in the deep margin of the Gulf of Lions, *Biogeosciences*, *10*(2), 1097–1116, doi:10.5194/bg-10-1097-2013.

Staehr, P. A., P. Henriksen, and S. Markager (2002), Photoacclimation of four marine phytoplankton species to irradiance and nutrient availability, *Mar. Ecol. Prog. Ser.*, *238*, 47–59, doi:10.3354/meps238047.

Tamburini C., M. Canals, X. Durrieu de Madron, L. Houpert, D. Lefèvre, and the ANTARES collaboration (2013), Deep-sea bioluminescence blooms after dense water formation at the ocean surface, *PLoS One*, *8*(7), e67523, doi:10.1371/journal.pone.0067523.

Taylor, J., and R. Ferrari (2011), Shutdown of turbulent convection as a new criterion for the onset of spring phytoplankton blooms, *Limnol. Oceanogr. Methods*, *56*, 2293–2307, doi:10.4319/lo.2011.56.6.2293.

Tengberg, A., E. Almroth, and P. Hall (2003), Resuspension and its effects on organic carbon recycling and nutrient exchange in coastal sediments: In situ measurements using new experimental technology, *J. Exp. Mar. Biol. Ecol.*, *285–286*, 119–142, doi:10.1016/S0022-0981(02)00523-3.

Uitz, J., H. Claustre, A. Morel, and S. B. Hooker (2006), Vertical distribution of phytoplankton communities in open ocean: An assessment based on surface chlorophyll, *J. Geophys. Res.*, *111*, C08005, doi:10.1029/2005JC003207.

Ulses, C., P.-A. Auger, K. Soetaert, P. Marsaleix, F. Diaz, L. Coppola, M. Herrmann, F. Kessouri, and C. Estournel (2016), Budget of organic carbon in the North-Western Mediterranean Open Sea over the period 2004–2008 using 3-D coupled physical-biogeochemical modeling, *J. Geophys. Res. Oceans*, *121*, 7026–7055, doi:10.1002/2016JC011818.

Waldman, R., et al. (2016), Estimating dense water volume and its evolution for the year 2012–2013 in the Northwestern Mediterranean Sea: An Observing System Simulation Experiment approach, *J. Geophys. Res. Oceans*, *121*, 6696–6716, doi:10.1002/2016JC011694.